Outage Performance of Uplink Pre-Amplified FSO Links Over Turbulence, Beam Wander, and Pointing Errors

M. P. Ninos, *Member, IEEE*, V. Spirito, G. Cossu, and E. Ciaramella, *Senior Member, IEEE*

***Abstract*— We analytically derive the outage probability (OP) estimation of a ground-to-satellite pre-amplified free-space optical (FSO) link. Our derivations analysis, for the first time, takes into account all the probabilistic impairments, i.e., atmospheric turbulence, beam wander and pointing errors (PEs). Novel, analytical closed-form expressions are extracted for the probability density function (PDF) and the cumulative distribution function (CDF) of the optical signal-to-noise ratio (OSNR) at the receiver pre-amplifier output. Furthermore, we conduct the asymptotic outage analysis in the high-OSNR regime, which provides insightful results for the uplink amplified FSO systems. Numerical OP results are presented for the case of a ground FSO link to a Geostationary Earth orbit (GEO) satellite under various turbulence conditions and misalignment scenarios. Finally, the whole outage analysis is verified by Monte Carlo simulations.**

***Index Terms*— Free-space optical communications, satellite communications, feeder uplink, optical amplifiers, atmospheric turbulence, beam wander, pointing errors, outage probability, asymptotic analysis.**

I. Introduction

OPTICAL satellite links are envisioned to play a key role in the future satellite networks and be integrated seamlessly with the terrestrial fiber networks [1]. Today, the backbone of satellite networks is being designed to rely on very-high-speed free-space optical (FSO) links [2], establishing uplink/downlink ground-to-space links as well as inter-satellite optical links and capitalizing on the same technology developed for fiber communications [1].

Among those, the most challenging links are the feeder uplinks, e.g., from an optical ground station (OGS) to a satellite. Those feeder links can suffer from major impairments due to the atmospheric layer. Even in good visibility conditions, atmospheric turbulence can provoke severe irradiance fluctuations in the received signal. Refractive and diffractive phenomena lead to undesired scintillation, spreading, and beam wandering [3], [4], [5]. In addition, feeder FSO systems require accurate alignment, so that any pointing jitter can significantly affect the system performance. As the diffraction-limited beam divergence angle is typically on the order of μrads, a pointing error (PE) higher than around 1 μrad severely impairs the link performance [6], [7].

Thus far, the performance of uplink FSO feeder links has been investigated in several letters. Firstly, the probability density function (PDF) under the assumption of two independent random variables (RVs) was derived [8], for various turbulence models and beam wander pointing jitter. The bit-error rate (BER) of heterodyne detection schemes and the probability of fade for an uplink system were investigated [4], [5], under the composite channel models of the Gamma ($\mathcal{G}$) and Gamma-Gamma ($\mathcal{GG}$) distributions with beam wander as two independent factors. The BER performance of an uplink FSO link with intensity modulation/direct detection (IM/DD) schemes was studied under the $\mathcal{GG}$ turbulence and beam wander-induced pointing error [9]. The development of a fading model with three independent RVs for $\mathcal{GG}$-modeled turbulence, beam wander and PEs in a horizontal link, was firstly launched in [10]. The same approach was then applied to an uplink FSO system with $\mathcal{G}$-modeled turbulence, beam wander and PEs [11].

However, future high-throughput FSO systems are being designed to encompass an optical erbium-doped fiber amplifier (EDFA) as a booster at the transmitter (TX) and, most importantly, as a pre-amplifier at the receiver (RX) [12]. EDFAs, which played a key role in high-speed fiber links, change the power-budget rules and make the power-sensitivity of the RX unimportant; when using them, the thermal and shot noises become negligible and the dominant source of noise is the amplified spontaneous emission (ASE), through the signal-ASE and ASE-ASE beating noise. Hence, in this regime the system performance is only determined by the optical signal-to-noise ratio (OSNR) at the pre-amplifier output [13]; this must exceed a minimum required value, which depends on the modulation format, bit rate and type of forward error correction (FEC) at the RX [13].

In this letter, we develop an analytical framework for the outage probability (OP) estimation of a ground-to-satellite pre-amplified FSO uplink. We take into account jointly the effects of atmospheric turbulence, beam wander, and PEs, each one treated as an independent RV. Under this assumption, we are able to independently assess the severity of each effect. The effect of scintillation is modelled by the $\mathcal{G}$ and $\mathcal{GG}$ distribution models, in order to provide a comprehensive assessment of every turbulence scenario. Specifically, in the weak turbulence regime, i.e. small zenith angles, the $\mathcal{G}$ distribution model is employed, while the $\mathcal{GG}$ model is selected for moderate to strong turbulence conditions [3], [4]. For the statistical evaluation of PEs, we employ the PE model of Toyoshima et al. [6], which is very accurate and appropriate for uplink

Manuscript received 28 September 2023; revised 26 October 2023; accepted 6 November 2023. Date of publication 8 November 2023; date of current version 12 December 2023. This work was partially supported by the European Union under the Italian National Recovery and Resilience Plan of NextGenerationEU, partnership on "Telecommunications of the Future" (PE00000001 - program "RESTART"). The associate editor coordinating the review of this letter and approving it for publication was C. Gong. *(Corresponding author: M. P. Ninos.)*

The authors are with Scuola Superiore Sant'Anna, Istituto di Tecnologie della Comunicazione, dell'Informazione e della Fotonica (TeCIP), 56124 Pisa, Italy (e-mail: m.ninos@santannapisa.it; v.spirito@santannapisa.it; g.cossu@santannapisa.it; e.ciaramella@santannapisa.it).

Digital Object Identifier 10.1109/LCOMM.2023.3331510

Fig. 1. Block diagram of the uplink ground-to-satellite pre-amplified FSO communication system.

laser communications and combined with the $\mathcal{G}$ and $\mathcal{GG}$ distribution models for the first time. For the beam wander effect, we consider the tracked beam case, i.e. tip-tilt adaptive optics (AO) pre-compensation [14], [15], and evaluate its impact as an independent source of spatial jitter by means of the root-mean-square (RMS) angular jitter. To the best of the authors' knowledge, this is the first attempt to evaluate the performance of an uplink FSO system with pre-amplification under the composite channel of $\mathcal{G}$ and $\mathcal{GG}$ distributions with beam wander and PEs, unlike the cases of [4], [5], and [9] where no PEs are considered or [11] where only the $\mathcal{G}$ distribution model is employed without pre-amplification. We evaluate its OP by means of new and tractable closed-form expressions for the PDF and the cumulative distribution function (CDF) of the OSNR at the pre-amplifier output. Finally, asymptotic analysis in the high-OSNR regime is conducted, providing insightful results for such laser communications systems.

II. System Model

In an amplified FSO system, the TX emits a signal, which is amplified by a booster EDFA and launched into free space by the TX telescope with average transmitted power P_0, as shown in Fig. 1. The received beam is collected by a second telescope, and P_{in} power is coupled into a single-mode fiber, amplified by a low-noise EDFA pre-amplifier and detected by a DD receiver or an array of balanced detectors.

As P_{in} is affected by the various effects described above, the composite channel coefficient I can be represented as a product of four independent factors, i.e. $I = I_l I_t I_b I_p$. Among them, I_l includes all the fixed losses of the link, i.e., extinction effects (absorption, scattering), losses due to free-space loss, TX/RX antenna gains and optics losses, fiber coupling loss etc. [3], [12], [16]. The other terms correspond to the three RVs of the channel, where I_t represents the scintillation effect, I_b the beam wander, and I_p the PEs [3], [4], [6]. For the sake of simplicity, we define the RV I_t' as $I_t' = I_l I_t$.

As known, the instantaneous OSNR at the EDFA output is related to the instantaneous power $P_{in} = P_0 I$ as [17]

$$\mathrm{OSNR}\left(I\right) = \frac{GP_0 I}{N_F\left(G-1\right)h\nu\Delta\nu} \tag{1}$$

where G is the EDFA gain, N_F is the pre-amplifier noise figure, h is Planck's constant, ν is the optical carrier frequency and $\Delta\nu$ is the resolution bandwidth, usually fixed at 12.5 GHz (0.1 nm) [13], without considering background noise.[1] Since the power fluctuations do not move the EDFA into saturation, the ASE spectral density and the EDFA gain are both constant, therefore the irradiance fluctuations produce a time-varying OSNR [17]. Note also that, in case of a wavelength division multiplexing (WDM) system, $P_0 I$ is the per-channel input power. Finally, the average OSNR is given by

$$\overline{\mathrm{OSNR}} = \frac{GP_0\mathbb{E}\{I\}}{N_F\left(G-1\right)h\nu\Delta\nu} \tag{2}$$

where $\mathbb{E}\{\cdot\}$ denotes the expected value of the enclosed, with $\mathbb{E}\{I\} = \mathbb{E}\{I_t'\}\mathbb{E}\{I_b\}\mathbb{E}\{I_p\}$. We highlight that modern optical systems exploit FEC; therefore, it is known that error-free transmission can be achieved at any $\overline{\mathrm{OSNR}}$ value greater than a threshold OSNR (OSNR_{th}), which can be linked directly to standard pre-FEC BER targets [13].

From the OGS to the satellite, the optical signal experiences the degradation effects of atmospheric turbulence. The $\mathcal{G}$ distribution is generally considered an accurate model for the uplink irradiance fluctuations for the weak turbulence regime [3]. Its mathematical representation is given as [3], [4]

$$f_{I_t',\mathcal{G}}\left(I_t'\right) = \frac{1}{\Gamma(m)I_t'}\left(\frac{mI_t'}{\mathbb{E}\{I_t'\}}\right)^m \exp\left(-\frac{mI_t'}{\mathbb{E}\{I_t'\}}\right) \tag{3}$$

where m is the $\mathcal{G}$ distribution parameter defined as $m = \left(\exp\left(\sigma^2_{\ln X} + \sigma^2_{\ln Y}\right) - 1\right)^{-1}$ [3, Eq. (24)], with $\sigma^2_{\ln X}$ and $\sigma^2_{\ln Y}$ denoting the small-scale and large-scale log-irradiance variances, related to the wavelength λ, the link distance L, the $C_n^2(h)$ turbulence profile and the beam parameters. The link distance is calculated as $L = (H - H_{OGS})\sec(\zeta)$, where H_{OGS} is the OGS altitude and H, ζ are the altitude and zenith angle of the satellite, respectively [3].

For the moderate to strong turbulence regime, it is well-known that the $\mathcal{GG}$ distribution accurately models the irradiance fluctuations. Its PDF is given as [3]

$$f_{I_t',\mathcal{GG}}(I_t') = \frac{2\left(I_t'\right)^{-1}}{\Gamma(a)\Gamma(b)}\left(\frac{abI_t'}{\mathbb{E}\{I_t'\}}\right)^{\frac{a+b}{2}} K_{a-b}\left(\sqrt{\frac{4abI_t'}{\mathbb{E}\{I_t'\}}}\right) \tag{4}$$

with $I_t' > 0$. $K_v(\cdot)$ denotes the modified Bessel function of the second kind with a, b being equal to $a = \left(\exp\left(\sigma^2_{\ln X}\right) - 1\right)^{-1}$ and $b = \left(\exp\left(\sigma^2_{\ln Y}\right) - 1\right)^{-1}$ [3, Eq. (22)]. The mean irradiance $\mathbb{E}\{I_t\}$ is calculated as [5, Eq. (13)]. For the $C_n^2(h)$, we use the modified Hufnagel-Valley model, which takes into account the OGS altitude above sea level [16].

Considering a Gaussian beam, where the azimuth and elevation angles are affected by independent Gaussian angular jitters with zero mean and identical angular variances, $\sigma^2_{\theta,j}$, the angular pointing error, θ, follows a Rayleigh distribution [6],

$$f_\theta\left(\theta\right) = \frac{\theta}{\sigma^2_{\theta,j}}\exp\left(-\frac{\theta^2}{2\sigma^2_{\theta,j}}\right), \quad \theta \geq 0 \tag{5}$$

where $j \in \{p, b\}$ stands for the case of misalignment either due to pointing errors or beam wander. Therefore, the instantaneous normalized irradiance for PEs, I_p, or beam wander, I_b, follows a beta distribution [6], given by

$$f_{I_p}\left(I_p\right) = qI_p^{q-1}, \quad 0 \leq I_p \leq 1 \tag{6a}$$

$$f_{I_b}\left(I_b\right) = \beta_w I_b^{\beta_w - 1}, \quad 0 \leq I_b \leq 1 \tag{6b}$$

where $q = \theta^2_{div}/4\sigma^2_{\theta,p}$, and $\beta_w = \theta^2_{div}/4\sigma^2_{\theta,b}$, respectively. The expected values of I_p and I_b are equal to $\mathbb{E}\{I_p\} = q\left(q+1\right)^{-1}$ and $\mathbb{E}\{I_b\} = \beta_w\left(\beta_w+1\right)^{-1}$ [6]. The half-angle

[1] In case background noise is considered [18], an additional noise term would be added to the denominator of Eq. (1), equal to GP_{bg}, where P_{bg} is the total background noise power collected by the receiver field of view (FoV) and can be directly from the Sun or any other celestial body. We consider a narrow FoV with a proper optical bandpass filter to eliminate the background radiation. In any other case, signal-background and background-ASE beating noise as well as shot noise should carefully be taken into account.

beam divergence, θ_{div}, is evaluated through the expression [19, Eq. (14)], and is connected with the beam spot radius W_0 at the TX and the diameter D_{TX} of the outer circular aperture of the TX telescope.

The PEs, which have a strong impact on the system performance, including the effect of wind speed, mechanical vibrations and errors in the pointing and tracking subsystem. All contribute to an RMS fashion, which amounts to a total pointing jitter, $\sigma_{\theta,p}$, ranging from 0.5 to 2 μrads for weak to strong influence [6], [7].

In addition, beam wander causes further beam movement. The RMS radial displacement due to beam wander, considering the case of a tracked beam where the Zernike tilt can ideally be subtracted [14], [15], is calculated as

$$\sigma^2_{\beta_w,\mathrm{rms}} = \left(\sqrt{\langle r_c^2\rangle} - T_z L\right)^2 \tag{7}$$

where $\langle r_c^2\rangle$ is the RMS beam wander displacement, calculated as $\langle r_c^2\rangle \approx 0.54\, L^2\,(\lambda/2W_0)^2\,(2W_0/r_0)^{5/3}$ for $H \gg 20$ km [3], and $T_z^2 = 0.3641\,(\lambda/D_R)^2\,(D_R/r_0)^{5/3}$ is the Zernike tilt angle variance [14], with D_R the receiver aperture diameter of the wave-front sensor and r_0 the Fried's parameter. The RMS angular displacement due to beam wander is defined as

$$\sigma_{\theta,b} = \frac{\sigma_{\beta_w,\mathrm{rms}}}{L}. \tag{8}$$

III. Outage Probability Analysis

A. Exact Closed-Form Expressions

The outage probability of the amplified uplink can be evaluated by having the CDF $F_{\mathrm{OSNR}}(x)$ of the time-varying OSNR. As a first step, we calculate the PDF $f_I(I)$ of the composite channel coefficient I, by using the multiplicative property of the Mellin transform (MT) [20]. Considering that the composite channel coefficient is $I = I_t' I_b I_p$, the product of the MTs of their PDFs is given by

$$\begin{aligned}\mathcal{M}\left(f_I(I)\,|\,s\right) = \mathcal{M}\left(f_{I_t'}(I_t')\,|\,s\right)\mathcal{M}\left(f_{I_p}(I_p)\,|\,s\right)\\ \times\,\mathcal{M}\left(f_{I_b}(I_b)\,|\,s\right),\end{aligned} \tag{9}$$

where $\mathcal{M}\left(f_X(x)\,|\,s\right)$ denotes the MT of the PDF $f_X(x)$ and s is a complex number in the s-domain. First, we calculate the MT for the $\mathcal{G}$ distribution, Eq. (3), which is obtained as

$$\mathcal{M}\left(f_{I_t',\mathcal{G}}(I_t')\,|\,s\right) = \left(\frac{m}{\mathbb{E}\{I_t'\}}\right)^{1-s}\frac{\Gamma(m+s-1)}{\Gamma(m)}. \tag{10}$$

The MT for the two beta distributions of Eqs. (6) for PEs and beam wander are calculated according to [20]

$$\mathcal{M}\left(f_{I_p}(I_p)\,|\,s\right) = q\frac{\Gamma(s+q-1)}{\Gamma(s+q)}, \tag{11a}$$

$$\mathcal{M}\left(f_{I_b}(I_b)\,|\,s\right) = \beta_w\frac{\Gamma(s+\beta_w-1)}{\Gamma(s+\beta_w)}. \tag{11b}$$

Consequently, we take the inverse MT of (9) as $f_I(I) = \frac{1}{2\pi j}\int_{c-j\infty}^{c+j\infty}\mathcal{M}\left(f_I(I)\,|\,s\right)I^{-s}ds$, and by virtue of Eqs. (10) and (11), we arrive at

$$\begin{aligned}f_{I,\mathcal{G}}(I) = \frac{m\beta_w q}{\mathbb{E}\{I_t'\}\Gamma(m)}\frac{1}{2\pi j}\int_{c-j\infty}^{c+j\infty}\frac{\Gamma(m+s-1)}{\Gamma(s+q)}\times\\ \times\,\frac{\Gamma(s+q-1)\,\Gamma(s+\beta_w-1)}{\Gamma(s+\beta_w)}\left(\frac{\mathbb{E}\{I_t'\}}{mI}\right)^s ds\end{aligned} \tag{12}$$

By noticing this Mellin-Barnes integral, the inverse MT is solved by using consecutively [21, Eqs. (6.422.19), (9.31.2), (9.31.5)], and calculating the PDF, $f_I(I)$, in a closed-form expression, as

$$f_{I,\mathcal{G}}(I) = \frac{\beta_w q}{\Gamma(m)\,I}G^{3,0}_{2,3}\left(\frac{mI}{\mathbb{E}\{I_t'\}}\,\middle|\,\begin{matrix}q+1,\beta_w+1\\ q,\beta_w,m\end{matrix}\right). \tag{13}$$

where $G^{m,n}_{p,q}\left(z\,|\,a_p;b_q\right)$ denotes the Meijer's G-function [22, Eq. (9.301)]. Following a RV transformation, we obtain the PDF of OSNR as follows

$$\begin{aligned}f_{\mathrm{OSNR},\mathcal{G}}(x) =\\ \frac{\beta_w q}{\Gamma(m)\,x}G^{3,0}_{2,3}\left(\frac{m\mathbb{E}\{I\}x}{\mathbb{E}\{I_t'\}\overline{\mathrm{OSNR}}}\,\middle|\,\begin{matrix}q+1,\beta_w+1\\ q,\beta_w,m\end{matrix}\right).\end{aligned} \tag{14}$$

The CDF of OSNR is derived in a closed-form solution, by means of the formula in [22, Eq. (26)] as

$$F_{\mathrm{OSNR},\mathcal{G}}(x) = \frac{\beta_w q}{\Gamma(m)}G^{3,1}_{3,4}\left(\frac{m\mathbb{E}\{I\}x}{\mathbb{E}\{I_t'\}\overline{\mathrm{OSNR}}}\,\middle|\,\begin{matrix}1,q+1,\beta_w+1\\ q,\beta_w,m,0\end{matrix}\right). \tag{15}$$

Thus, the OP can be evaluated at a specified OSNR_{th}, as $\mathrm{OP} = F_{\mathrm{OSNR},\mathcal{G}}(\mathrm{OSNR}_{th})$ [13].

Concerning the case of the $\mathcal{GG}$ distribution with beam wander and PEs, we follow similar steps as analysed above. Specifically, the MT of the $\mathcal{GG}$ distribution, Eq. (4), is given as [10]

$$\mathcal{M}\left(f_{I_t',\mathcal{GG}}(I_t')\,|\,s\right) = \frac{\Gamma(a+s-1)\,\Gamma(b+s-1)}{\Gamma(a)\,\Gamma(b)\left(\frac{ab}{\mathbb{E}\{I_t'\}}\right)^{s-1}}. \tag{16}$$

Replacing (16) into (9) and using Eqs. (11), the inverse MT of the product can readily be calculated following the steps as in (12). Thus, the PDF of the total channel coefficient I, for the case of $\mathcal{GG}$ model, is calculated as

$$f_{I,\mathcal{GG}}(I) = \frac{\beta_w q}{\Gamma(a)\,\Gamma(b)\,I}G^{4,0}_{2,4}\left(\frac{abI}{\mathbb{E}\{I_t'\}}\,\middle|\,\begin{matrix}\beta_w+1,q+1\\ q,\beta_w,a,b\end{matrix}\right). \tag{17}$$

The PDF of OSNR for the $\mathcal{GG}$ turbulence case with beam wander and PEs is derived accordingly as

$$\begin{aligned}f_{\mathrm{OSNR},\mathcal{GG}}(x)\\ = \frac{\beta_w q}{\Gamma(a)\,\Gamma(b)\,x}G^{4,0}_{2,4}\left(\frac{ab\mathbb{E}\{I\}x}{\mathbb{E}\{I_t'\}\overline{\mathrm{OSNR}}}\,\middle|\,\begin{matrix}q+1,\beta_w+1\\ q,\beta_w,a,b\end{matrix}\right),\end{aligned} \tag{18}$$

while the corresponding CDF of OSNR for the $\mathcal{GG}$ model is deduced as

$$\begin{aligned}F_{\mathrm{OSNR},\mathcal{GG}}(x)\\ = \frac{\beta_w q}{\Gamma(a)\,\Gamma(b)}G^{4,1}_{3,5}\left(\frac{ab\mathbb{E}\{I\}x}{\mathbb{E}\{I_t'\}\overline{\mathrm{OSNR}}}\,\middle|\,\begin{matrix}1,q+1,\beta_w+1\\ q,\beta_w,a,b,0\end{matrix}\right).\end{aligned} \tag{19}$$

B. Asymptotic Analysis

In addition to the closed-form expressions of Eqs. (15) and (19), we provide an asymptotic analysis, which is valid when $\overline{\mathrm{OSNR}} \to \infty$. In order to derive an asymptotic approximation of (15), we use the expansion formula for the Meijer's

G-function in terms of the generalized hypergeometric function ${}_qF_p\left(a_q, b_p; z\right)$ as given in [21, Eq. (9.303)], where

$$z_{\mathcal{G}} = \frac{m\mathbb{E}\{I\}x}{\mathbb{E}\{I_t'\}\overline{\text{OSNR}}}. \tag{20}$$

When $\overline{\text{OSNR}} \to \infty$, i.e. $z_{\mathcal{G}} \ll 1$, then ${}_qF_p\left(a_q, b_p; z_{\mathcal{G}}\right) \to 1$ and (15) is approximated as follows

$$F_{\text{OSNR},\mathcal{G}}(x) \underset{\overline{\text{OSNR}}\to\infty}{\approx} \underbrace{\frac{\beta_w q z_{\mathcal{G}}^m}{m\left(q-m\right)\left(\beta_w - m\right)\Gamma\left(m\right)}}_{\mathcal{J}_{1,\mathcal{G}}} + \underbrace{\frac{q\Gamma\left(m-\beta_w\right)z_{\mathcal{G}}^{\beta_w}}{\left(q-\beta_w\right)\Gamma\left(m\right)}}_{\mathcal{J}_{2,\mathcal{G}}} + \underbrace{\frac{\beta_w\Gamma\left(m-q\right)z_{\mathcal{G}}^{q}}{\left(\beta_w - q\right)\Gamma\left(m\right)}}_{\mathcal{J}_{3,\mathcal{G}}}. \tag{21}$$

Following the same procedure as described above, we obtain the asymptotic expression of (19) as follows

$$\begin{aligned} &F_{\text{OSNR},\mathcal{GG}}(x) \\ &\underset{\overline{\text{OSNR}}\to\infty}{\approx} \underbrace{\frac{\beta_w q\Gamma\left(b-a\right)z_{\mathcal{GG}}^{a}}{\left(\beta_w - a\right)\left(q-a\right)\Gamma\left(b\right)\Gamma\left(1+a\right)}}_{\mathcal{J}_{1,\mathcal{GG}}} \\ &+ \underbrace{\frac{q\Gamma\left(a-\beta_w\right)\Gamma\left(b-\beta_w\right)z_{\mathcal{GG}}^{\beta_w}}{\left(q-\beta_w\right)\Gamma\left(a\right)\Gamma\left(b\right)}}_{\mathcal{J}_{2,\mathcal{GG}}} + \underbrace{\frac{\beta_w\Gamma\left(a-q\right)\Gamma\left(b-q\right)z_{\mathcal{GG}}^{q}}{\left(\beta_w - q\right)\Gamma\left(a\right)\Gamma\left(b\right)}}_{\mathcal{J}_{3,\mathcal{GG}}} \\ &+ \underbrace{\frac{\beta_w q\Gamma\left(a-b\right)z_{\mathcal{GG}}^{b}}{\left(\beta_w - b\right)\left(q-b\right)\Gamma\left(a\right)\Gamma\left(1+b\right)}}_{\mathcal{J}_{4,\mathcal{GG}}}, \end{aligned} \tag{22}$$

where $z_{\mathcal{GG}}$ is equal to

$$z_{\mathcal{GG}} = \frac{ab\mathbb{E}\{I\}x}{\mathbb{E}\{I_t'\}\overline{\text{OSNR}}}. \tag{23}$$

From Eqs. (21) and (22), we notice the asymptotic behaviour of the OP, as $\text{OP} \approx \left(\mathcal{O}_c\overline{\text{OSNR}}\right)^{-\mathcal{O}_d}$, where $\mathcal{O}_d$ denotes the outage diversity order. Thus, the outage diversity order, for the $\mathcal{G}$ and $\mathcal{GG}$ turbulence models, is given as

$$\mathcal{O}_{d,\mathcal{G}} = \min\left(q, \beta_w, m\right), \tag{24a}$$

$$\mathcal{O}_{d,\mathcal{GG}} = \min\left(q, \beta_w, a, b\right). \tag{24b}$$

IV. Numerical Results

With the aid of the closed-form expressions of (15), (19) and the asymptotic expressions of (21) and (22), we provide numerical results for the OP estimation of an uplink-to-Geostationary Earth orbit (GEO) satellite (altitude $H = 35786$ km) FSO link. For all the results, we consider $\text{OSNR}_{th} = 10$ dB. We assume an optical wavelength $\lambda = 1.55$ μm, the beam spot radius $W_0 = 122$ mm, TX telescope and sensor diameters $D_{TX}, D_R = 270$ mm, and the phase front radius $F_0 \to \infty$. The RMS wind speed is $v_{\text{rms}} = 21$ m/s and we assume moderate and strong ground level turbulence with $C_n^2\left(0\right) = 1.7 \times 10^{-14}$ m$^{-2/3}$ and $C_n^2\left(0\right) = 1.7 \times 10^{-13}$ m$^{-2/3}$, considered as realistic nighttime and daytime conditions, respectively. We assume two zenith angles where for $\zeta = 30^o$ the $\mathcal{G}$ model is employed, whilst for $\zeta = 60^o$ the $\mathcal{GG}$ distribution is used. All the numerical results are accompanied by extensive Monte Carlo simulations using 2×10^6 realizations.

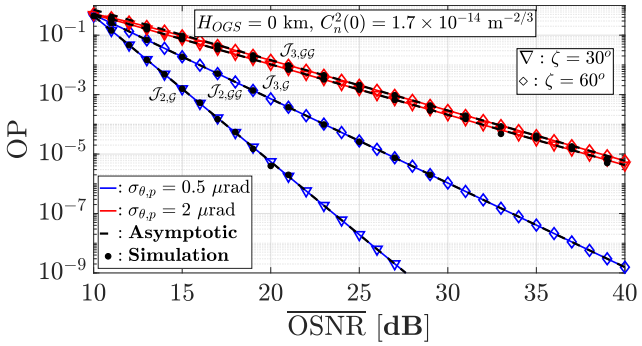

Fig. 2. Outage probability vs. $\overline{\text{OSNR}}$, for zenith angle $\zeta = 30^o$ or 60^o, and PEs of $\sigma_{\theta,p} = 0.5$ or 2 μrad, when $H_{OGS} = 0$ km and nighttime conditions.

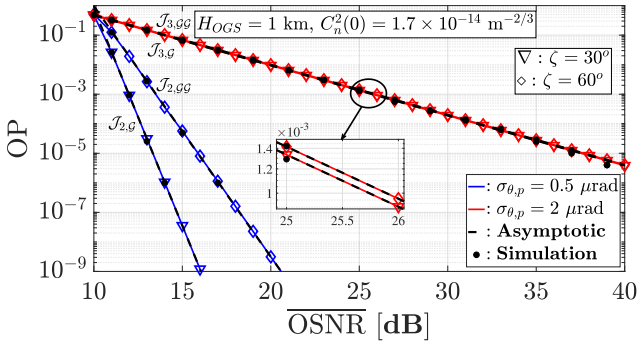

Fig. 3. Outage probability vs. $\overline{\text{OSNR}}$, for zenith angle $\zeta = 30^o$ or 60^o, and PEs of $\sigma_{\theta,p} = 0.5$ or 2 μrad, when $H_{OGS} = 1$ km and nighttime conditions.

In Fig. 2 the OP is shown versus $\overline{\text{OSNR}}$ for the case of an OGS at $H_{OGS} = 0$ km. The blue curves refer to weak PEs, whilst the red curves refer to quite high PEs. Also, different ζ values are assumed, i.e. 30^o (triangles) and 60^o (diamonds). It can clearly be noticed that very low OP is obtained at quite acceptable $\overline{\text{OSNR}}$ values (e.g. 20 dB). Furthermore, the turbulence impact is predominant when PEs are low, observing the remarkable impact of ζ. If PEs are high, its statistical impact dominates over all other effects and much higher $\overline{\text{OSNR}}$ values are needed to achieve the same outage performance. All these curves are accompanied by asymptotic results, plotted in the whole range of $\overline{\text{OSNR}}$ by using only the dominant term $\mathcal{J}_{\chi,\chi}$ which in turn determines the diversity order in the high-OSNR regime. We can clearly notice the tightness of the asymptotics even in the low to medium OSNR regime, emulating perfectly the closed-form results. In Fig. 3 the OP results are illustrated for similar conditions, but for $H_{OGS} = 1$ km. In this case, we obtain a lower impact of atmospheric effects. This is clearly noticeable, however, only for weak PEs of blue curves. For any $\overline{\text{OSNR}}$ value, the corresponding OP is acceptable for both values of ζ. The asymptotic curves follow firmly the closed-form ones with the use of $\mathcal{J}_{2,\mathcal{G}}$ and $\mathcal{J}_{2,\mathcal{GG}}$ terms, respectively. However, the OP corresponding to the red curves ($\sigma_{\theta,p} = 2$ μrad) shows only minor improvements between the two zenith angles. This confirms that in this regime the system outage is largely determined by PEs, verified also by the asymptotic terms of $\mathcal{J}_{3,\mathcal{G}}$ and $\mathcal{J}_{3,\mathcal{GG}}$ in the whole $\overline{\text{OSNR}}$ range.

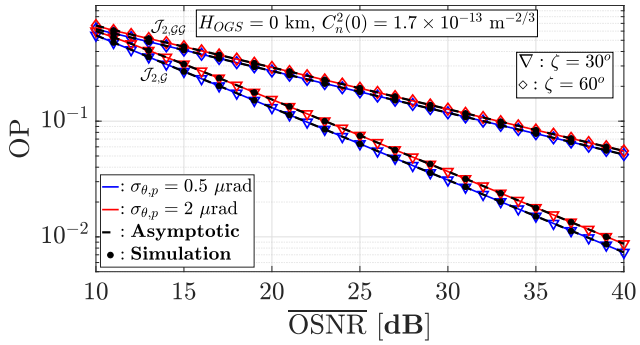

Fig. 4. Outage probability vs. $\overline{\text{OSNR}}$, for zenith angle $\zeta = 30^o$ or 60^o, and PEs of $\sigma_{\theta,p} = 0.5$ or 2 μrad, when $H_{OGS} = 0$ km and daytime conditions.

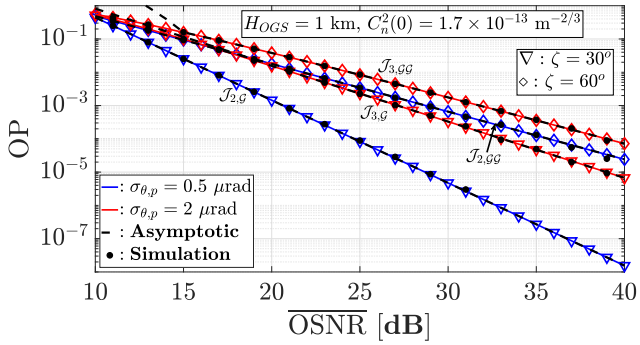

Fig. 5. Outage probability vs. $\overline{\text{OSNR}}$, for zenith angle $\zeta = 30^o$ or 60^o, and PEs of $\sigma_{\theta,p} = 0.5$ or 2 μrad, when $H_{OGS} = 1$ km and daytime conditions.

Finally, Figs. 4 and 5, present the OP results considering strong ground level turbulence, which correspond to realistic daytime conditions, for the cases of OGS height at $H_{OGS} = 0$ km and $H_{OGS} = 1$ km, respectively. For the case of $H_{OGS} = 0$ km (Fig. 4), we notice the performance degradation across all the range of $\overline{\text{OSNR}}$, where neither low nor high satellite-zenith-angle FSO uplinks can be implemented. The asymptotic results are plotted by using only the $\mathcal{J}_{2,\mathcal{G}}$ and $\mathcal{J}_{2,\mathcal{GG}}$ terms, from low to high $\overline{\text{OSNR}}$, revealing the tremendous impact of beam wander effect under such conditions. On the other hand, in the case of $H_{OGS} = 1$ km (Fig. 5), it is clearly observed that the OP performance can be improved and retained at acceptable levels. Again, under strong PEs influence the performance is strongly affected and $\overline{\text{OSNR}}$ values above 27 dB are required for acceptable performance. For the case of weak PEs, we observe how critical becomes the influence of ζ on the uplink FSO system performance. The asymptotic results are plotted by using all the terms of (21) and (22) and some deviations are noticed, especially in the low OSNR regime.

V. Conclusion

This letter provides a comprehensive and analytical performance estimation of an optically pre-amplified ground-to-satellite FSO link by means of novel and tractable closed-form and asymptotic OP analysis in terms of the OSNR at the receiver end. We take into account the $\mathcal{G}$ and the $\mathcal{GG}$-modeled turbulence in conjunction with beam wander and PEs, each one of them as an independent RV. The derived mathematical framework can be employed and extended to a plethora of uplink scenarios, including the design of WDM-FSO systems by means of a few simple generalizations.

References

[1] J. Perdigues et al., "HYDRON: The ESA initiative towards optical networking in space," in *Proc. Eur. Conf. Opt. Commun. (ECOC)*, Bordeaux, France, Sep. 2021, pp. 1–4.
[2] E. Ciaramella et al., "1.28 terabit/s (32 × 40 Gbit/s) wdm transmission system for free space optical communications," *IEEE J. Sel. Areas Commun.*, vol. 27, no. 9, pp. 1639–1645, Dec. 2009.
[3] L. C. Andrews, R. L. Phillips, R. J. Sasiela, and R. Parenti, "PDF models for uplink to space in the presence of beam wander," *Proc. SPIE*, vol. 655109, May 2007, Art. no. 655109.
[4] H. Sandalidis, "Performance analysis of a laser ground-station-to-satellite link with modulated gamma-distributed irradiance fluctuations," *J. Opt. Commun. Netw.*, vol. 2, no. 11, pp. 938–943, Nov. 2010.
[5] H. G. Sandalidis, "Performance of a laser Earth-to-satellite link over turbulence and beam wander using the modulated gamma–gamma irradiance distribution," *Appl. Opt.*, vol. 50, no. 6, pp. 952–961, Feb. 2011.
[6] M. Toyoshima, T. Jono, K. Nakagawa, and A. Yamamoto, "Optimum divergence angle of a Gaussian beam wave in the presence of random jitter in free-space laser communication systems," *J. Opt. Soc. Amer. A, Opt. Image Sci.*, vol. 19, no. 3, pp. 567–571, Mar. 2002.
[7] M. Toyoshima et al., "Ground-to-satellite laser communication experiments," *IEEE Aerosp. Electron. Syst. Mag.*, vol. 23, no. 8, pp. 10–18, Aug. 2008.
[8] K. Kiasaleh, "On the probability density function of signal intensity in free-space optical communications systems impaired by pointing jitter and turbulence," *Proc. SPIE*, vol. 33, no. 11, pp. 3748–3757, Nov. 1994.
[9] A. Viswanath, V. K. Jain, and S. Kar, "Analysis of Earth-to-satellite free-space optical link performance in the presence of turbulence, beam-wander induced pointing error and weather conditions for different intensity modulation schemes," *IET Commun.*, vol. 9, no. 18, pp. 2253–2258, Dec. 2015.
[10] M. P. Ninos, P. Mukherjee, C. Psomas, and I. Krikidis, "Full-duplex DF relaying with parallel hybrid FSO/RF transmissions," *IEEE Open J. Commun. Soc.*, vol. 2, pp. 2502–2515, 2021.
[11] E. Elsaidy and T. Rakia, "A unified performance analysis of OGS-to-satellite FSO UpLink under turbulence and beam wander," in *Proc. 5th Int. Conf. Commun., Signal Process., Appl. (ICCSPA)*, Cairo, Egypt, Dec. 2022, pp. 1–6.
[12] D. Giggenbach et al., "Preliminary results of terabit-per-second long-range free-space optical transmission experiment THRUST," *Proc. SPIE*, vol. 9647, Oct. 2015, Art. no. 96470H.
[13] P. J. Winzer and R.-J. Essiambre, "Advanced optical modulation formats," *Proc. IEEE*, vol. 94, no. 5, pp. 952–985, May 2006.
[14] R. J. Sasiela and J. D. Shelton, "Transverse spectral filtering and Mellin transform techniques applied to the effect of outer scale on tilt and tilt anisoplanatism," *J. Opt. Soc. Amer. A, Opt. Image Sci.*, vol. 10, no. 4, pp. 646–660, 1993.
[15] J. Osborn, M. J. Townson, O. J. D. Farley, A. Reeves, and R. M. Calvo, "Adaptive optics pre-compensated laser uplink to LEO and GEO," *Opt. Exp.*, vol. 29, no. 4, pp. 6113–6132, Feb. 2021.
[16] S. Dimitrov, R. Barrios, B. Matuz, G. Liva, R. Mata-Calvo, and D. Giggenbach, "Digital modulation and coding for satellite optical feeder links with pre-distortion adaptive optics," *Int. J. Satell. Commun. Netw.*, vol. 34, no. 5, pp. 625–644, Sep. 2016.
[17] G. P. Agrawal, *Fiber-Optic Communications Systems*, 3rd ed. Hoboken, NJ, USA: Wiley, 2002.
[18] N. S. Kopeika and J. Bordogna, "Background noise in optical communication systems," *Proc. IEEE*, vol. 58, no. 10, pp. 1571–1577, Oct. 1970.
[19] E. M. Drège, N. G. Skinner, and D. M. Byrne, "Analytical far-field divergence angle of a truncated Gaussian beam," *Appl. Opt.*, vol. 39, no. 27, pp. 4918–4925, Sep. 2000.
[20] B. Epstein, "Some applications of the Mellin transform in statistics," *Ann. Math. Statist.*, vol. 19, no. 3, pp. 370–379, Sep. 1948.
[21] I. S. Gradshteyn and I. M. Ryzhik, *Table of Integrals, Series, and Products*, 7th ed. Burlington, MA, USA: Elsevier, 2007.
[22] V. S. Adamchik and O. I. Marichev, "The algorithm for calculating integrals of hypergeometric type functions and its realization in REDUCE system," in *Proc. Int. Symp. Symbolic Algebr. Comput.*, Tokyo, Japan, Jul. 1990, pp. 212–224.

Open Access funding provided by 'Scuola Superiore "S.Anna" di Studi Universitari e di Perfezionamento' within the CRUI CARE Agreement